Bayesian Morphological Clock versus Parsimony: An Insight into the Relationships and Dispersal Events of Postvacuum Cricetidae (Rodentia, Mammalia)

Raquel López-Antoñanzas, Pablo Peláez-Campomanes

Bayesian Morphological Clock versus Parsimony: An insight into the relationships and dispersal events of postvacuum Cricetidae (Rodentia, Mammalia)

Raquel López-Antoñanzas[1,2]* and Pablo Peláez-Campomanes[2]

[1]Laboratoire de Paléontologie, Institut des Sciences de l'Évolution (ISE-M, UMR 5554, CNRS/UM/IRD/EPHE), Université de Montpellier, Montpellier, France

[2]Departamento de Paleobiología, Museo Nacional de Ciencias Naturales-CSIC, Madrid, Spain

*Corresponding author email: raquel.lopez-antonanzas@umontpellier.fr

ABSTRACT

Establishing an evolutionary timeline is fundamental for tackling a great variety of topics in evolutionary biology, including the reconstruction of patterns of historical biogeography, coevolution and diversification. However, the tree of life is pruned by extinction and molecular data cannot be gathered for extinct lineages. Until recently methodological challenges have prevented the application of tip-dating Bayesian approaches in morphology-based fossil-only datasets. Herein, we present a morphological dataset for a group of cricetid rodents to which we apply an array of methods fairly new in palaeontology that can be used by palaeontologists for the analysis of entirely extinct clades. We compare the tree topologies obtained by traditional parsimony, time-calibrated and non-calibrated Bayesian inference phylogenetic approaches and calculate stratigraphic congruence indices for each. Bayesian tip-dated clock methods outperform parsimony in the case of our dataset, which includes

highly homoplastic morphological characters. Regardless, all three topologies support the monophyly of Megacricetodontinae, Democricetodontinae and Cricetodontinae. Dispersal and speciation events inferred through Bayesian Binary Markov chain Monte Carlo and biodiversity analyses provide evidence for a correlation between biogeographic events, climatic changes and diversification in cricetids.

Keywords: Cricetidae, Miocene, Bayesian tip-dating, morphological clock, parsimony, STRAP, palaeobiogeography, palaeoecology, palaeobiodiversity

The fossil record is our only resource for providing a deep-time perspective of ecosystem processes and, therefore, for understanding the dynamics that have shaped our current biota. It is increasingly clear that fossil data are fundamental to infer species diversification, particularly extinction rates (Mitchell et al., 2019). Despite the fact that morphological phylogenetics have been increasingly marginalised in the last decades, morphological data remain the only available information to reconstruct evolutionary scenarios and reconcile the fossil record with molecular trees (Wright 2017; Lee and Palci 2015). The importance of morphological phylogenetics for dating rigorously the tree of life is now widely recognized and has been bolstered by recent methodological developments (Hunt and Slater 2016; Lee and Palci 2015; Wright 2017). Recent developments applying Bayesian methods using fossil taxa as tips, what is called the morphological clock, have been revitalizing the use of morphological data to elucidate the dynamics of evolution over time and across the tree of life (Varela et al. 2019; Simões et al. 2018, 2020a). While these analyses are usually carried out with data from both fossils and extant taxa, a very interesting application of this methodology is that it can be employed with data from extinct clades only, which adds to the palaeontologist's toolbox another method of reconstructing the evolution. This makes it now possible to compare phylogenies of extinct taxa obtained by means of evolutionary models with those resulting from maximum parsimony, which is the most widely applied method for analysing morphological data.

Time provides palaeontologists with a unique perspective on phylogeny. A few methods to integrate stratigraphic data with parsimony analyses were already available in the 90's (Wagner, 1995; Fisher, 1994). However, palaeontologists had to devote considerable time and effort in the process of calibrate them manually because of the lack of user-friendly software facilitating time-calibration of cladograms. Moreover, depending on the number of taxa included in the dataset palaeontologists have to infer the distribution of morphological

characters without the inclusion of temporal data, with the subsequent loss of information. Parsimony was until recently the only way for palaeontologists to analyse their morphological fossil datasets. However, since the introduction of Bayesian tip-dated phylogenetic methods, which were first applied with uniform tree prior (Ronquist et al. 2012) and then with fossilized birth-death (FBD) tree priors (Stadler 2010; Heath et al. 2014), the inclusion of stratigraphic data into phylogenetic analyses boomed. The development of tip-dating with FBD tree priors that allow fossil species to be included as terminal tips has been particularly useful for palaeontologists. Recent numerical methods such as PaleoTree (Bapst, 2012, 2014) or STRAP (Stratigraphic Tree Analysis for Palaeontology) (Bell and Lloyd 2014) allow phylogenies resulting from both parsimony and Bayesian analyses of fossil taxa to be dated. The package STRAP allows besides to assess their stratigraphic congruence (Bell and Lloyd 2014; O'Connor and Wills 2016; King and Beck 2019; King 2021). So, the development of all these comparative methods have promoted the revival of phylogenetic analysis incorporating stratigraphic data and the testing of different techniques of phylogenetic reconstruction using morphological data (Bell and Lloyd 2014; Sansom et al., 2018; King 2021). This provides palaeontologists with a golden opportunity to expand considerably their research toolkit.

Over the years, the development of numerical, parsimony and Bayesian methods to determine trees has resulted in an intense study of certain clades (Benton 2015). However, the most striking aspect of rodent palaeophylogenetics is the low ratio of phylogenetic hypotheses to species number. In fact, few comprehensive morphological phylogenetic analyses have been carried out for these mammals and none has been performed applying morphological clock methods. Nonetheless, rodents have an excellent fossil record and their dentition provides an ideal dataset to characterize phenotypic variation and calibrating divergence time analyses. The present work rests on cricetids, which are an important group of rodents because they include representatives involved in the first radiation of modern rodents in Eurasia during the Miocene.

They probably gave rise to other important lineages, such as arvicolines (voles), cricetines (hamsters) and even murines (mice). The Miocene comprises the first phase in the development of modern terrestrial ecosystems. This is a time interval that witnessed enormous geographical and environmental changes and during which the mammal record experienced a major turnover and successive dispersal events. Cricetids possibly appeared in China in Middle Eocene times (Tong 1992). After an initial radiation in Central Asia, the group expanded in Western Europe just after the "Grande Coupure" (Stehlin, 1910), when the Turgaï Strait dried out and a land bridge between Europe and Asia was established. They prospered in Europe during the Oligocene but primitive cricetids disappeared before the arrival of the more derived, typical Miocene ones. The time interval devoid of cricetids has been called the "cricetid vacuum" by Daams and Freudenthal (1989). Post-vacuum cricetids are known worldwide and under various morphologies since Miocene times, but their evolutionary history is poorly known. The biogeographic relationships and phylogenetic affinities of cricetid species with one another need to be studied in a time-scaled phylogenetic framework. This work aims to clear up the phylogenetic relationships and estimate divergence times of postvacuum cricetids to elucidate their origin and the dispersal events they underwent by applying parsimony and Bayesian methods to an array of important extinct lineages of Miocene cricetids from Europe, the Middle East and Asia. Moreover, the different approaches we use are assessed on the basis of the stratigraphic coherence of the resulting topologies in order to arrive at an informed opinion on which method is most likely to yield the most accurate results in the phylogenetic analyses of palaeontological (morphological) dataset.

MATERIAL AND METHODS

Material

The systematic study presented below is based on the examination of original specimens listed in Supplementary Tab. S1 provided in the Supplementary Information available in the

Dryad data repository https://datadryad.org/stash/share/Dmda4GGW64PE8-c4fZiwP2VpbnTlTZpWm4PRSm5L20Q.

First, second and third lower molars are designated as m1, m2 and m3, respectively and first, second and third upper molars as M1, M2 and M3, respectively.

Maximum Parsimony Analyses

Implied weights maximum parsimony analysis—A total of 82 phylogenetically informative dental characters from 74 taxa have been coded. The data matrix (Supplementary file S1 available on Dryad) has been built using Mesquite 3.04 (Maddison & Maddison 2009) and the analysis ran in TNT v.1.5 (Goloboff et al. 2003) using the new technology search algorithms and the implied weighting algorithm (Supplementary file S2 available on Dryad) (Goloboff et al. 2008). New technology search algorithms are recommended for large datasets because they allow the sampling of trees from a broader spectrum of local optima (Goloboff et al. 1999). Tree searches have been carried out using 1,000 initial trees by random addition sequences with 100 iterations or rounds for each of the four NTS algorithms: sectorial search, ratchet, drift and tree fusing. The analysis has been performed with K = 10 and collapsing all branches with support = 0. *K* values larger than the default (3.0) are more accurate to perform analyses for large datasets (Goloboff et al. 2017). The number of suboptimal trees to be retained was set at 10 and the relative fit difference at 0.1. The final output trees (22 MPTs+suboptimal trees) have been filtered for all the most parsimonious trees (MPTs). A total of 3 MPT with a length of 487 steps, a Consistency Index (CI) of 0.261 and a Retention Index (RI) of 0.765 have been obtained and have been used to calculate the strict consensus tree (488 steps) (Supplementary Figure S1 available on Dryad). Character 1, length of the M1, has been treated as additive. Branch support have been estimated through two complementary indices: Bremer Support (Bremer 1994) and Relative Bremer Support (Goloboff and Farris 2001).

Equal weights maximum parsimony analysis—The analysis has been also carried out with TNT using equal weights. Tree searches have been conducted as performed for the implied weighting parsimony analysis. The final output trees (440 MPTs+suboptimal trees) have been filtered for all the most parsimonious trees (MPTs). A total of 375 MPT with 479 steps, a Consistency Index (CI) of 0.265 and a Retention Index (RI) of 0.767 have been obtained and have been used to calculate the strict (530 steps) and majority (488 steps) consensus trees (Supplementary Figures S2 and S3 available on Dryad).

Bayesian inference analyses

Analyses have been carried out using Mr. Bayes v.3.2.6 (Ronquist et al. 2012) and the BEAST2 package (Bouckaert R., et al. (2014) using the CIPRES Science Gateway v.3.3 (Miller et al., 2010).

Non-clock Bayesian analysis—The analysis has been performed with Mr. Bayes v.3.2.6 (Ronquist et al. 2012). The morphological dataset (Supplementary file S1 available on Dryad) has been analysed with the MkV model (Lewis, 2001) under the γ model, 30 million generations and four independent runs. Convergence of independent runs is assessed by an average standard deviation of split frequencies of 0.0148, by an average potential scale reduction factors (PSRF) of 1 for all parameters and an effective sample size (ESS) greater than 200 for each parameter.

Time-calibrated relaxed-clock Bayesian inference analysis—The analysis has been performed in BEAST2 package (Bouckaert R. et al. 2014) (Supplementary file S3 available on Dryad). The Mkv model (Lewis 2001) has been used, with a gamma distribution with four rate categories to account for rate variation across sites. The prior on the gamma shape parameter is an exponential distribution. Following Simões et al. (2020a), the morphological dataset has

been analysed using the fossilized birth-death tree model with sampled ancestors (FBD-SA) (Stadler 2010), under relaxed-clock models, 30 million generations and four independent runs with the initial 30% of samples removed as "burn-in". The relaxed-clock model is the independent γ rate relaxed-clock model, which is a continuous uncorrelated relaxed-clock model using a gamma distribution to assess clock rate variation across lineages (Simões et al 2018). It is compatible with the fossilized birth–death tree model. The base clock rate has been given an informative prior that derived from the undated Bayesian inference analysis: the median value for tree height (TL) in substitutions from the entire posterior trees sample (TL=9.9825) divided by the age of the tree (37.6 Ma), which is based on the median of the distribution for the root prior. So, the prior is: 9.9825/37.6=0.265. In contrast to Mr. Bayes, BEAST 2 does not allow different modelling strategies for how extant taxa are sampled and assumes a random sampling strategy (Simões et al, 2020b), which is unimportant in studies that do not include extant species. Our calibrations have been based on tip dating, which accounts for the uncertainty in the placement of fossil taxa and avoids the issue of bound estimates for node-based age calibrations (Ronquist et al. 2016, Simões et al. 2018). It has been substantiated that sampling fossil ages instead of fixing them to the midpoint within their stratigraphic age range avoids biases in divergence time estimations (Barido-Sotani et al., 2019). Thus, the fossil ages used in this work for tip dating correspond to the uniform prior distributions on the age range of the stratigraphic occurrence of the fossils. The age of the root has been set with a soft lower bound. The minimum age of the root corresponds to the oldest age for the oldest fossil belonging to *Eucricetodon* and the maximum root has been set at 41.2 Ma (Middle/Late Eocene boundary), which is the maximum soft age for the clade Eucricetodontinae. Conditioning on rho has not been possible because the data set of the analysis only contains extinct taxa so we have conditioned on the root and on sampling (Supplementary file S3 available on Dryad). An effective sample size (ESS) greater than 200 for the main parameters assesses the convergence of independent runs.

Stratigraphic congruence

To assess the stratigraphic congruence of the parsimony and Bayesian inference-derived phylogenies resulting from our analyses we used the package STRAP for R with the default number of permutations (1000) (Bell and Lloyd, 2014). We have obtained the following stratigraphic fit indices: MIG (minimum implied gap (Norell and Novacek, 1992; Norell et al. 1992)), SCI (Stratigraphy Consistency Index (Huelsenbeck 1994)), RCI (Relative Completeness Index (Benton and Storrs 1994)), GER (Gap Excess Ratio (Wills 1999)), MSM* (modified Manhattan Stratigraphic Measure (Pol, 2001)) and Wills' modifications of GER (GERt and GER*, Wills et al. (2008)). MIG provides the sum of the branch lengths excluding tip durations (the sum of the ghost ranges), SCI provides the proportion of nodes that are stratigraphically congruent in a tree, RCI provides the measure of the extent of observed ranges of taxa and the sum of the ghost ranges, MSM* corresponds to MIG for the maximally stratigraphically consistent possible tree divided by the actual MIG and GER to MIG minus the best possible stratigraphic fit, scaled by the contrast between the best and worst fit values (Lloyd and Bell, 2014; Wright and Lloyd, 2020)). SCI, GER, GERt, and MSM* scale between 0.0 (least congruent) and 1.0 (most congruent) (O'Connor and Wills 2016; Wright and Lloyd, 2020). Additionally, the program provides the significance test for those measurements (p.SCI, p.RCI, p.GER, and p.MSM*) as well as a combined fit and significance test measure (GER*and GERt) (Bell and Lloyd 2014). The p-values indicate the probability of the null hypothesis, which indicates random tree topology. So, very small p-values will indicate a significantly good fit to stratigraphy (Bell and Lloyd 2014).

Biogeographic Inference using Reconstruct Ancestral State in Phylogenies

In order to infer historical biogeography we have applied RASP 4.2 (Yu et al. 2015), a method to reconstruct ancestral geographical distributions using a combination of phylogenetic and geographical information. Bayesian Binary Markov chain Monte Carlo (BBM) method for

ancestral state has been performed on the Maximum Clade Credibility Tree (MCCT) in RASP 4.2 (Yu et al. 2015). BBM calculates the probabilities of ancestral ranges using the probabilities of each unit area generated by MrBayes (Yu et al. 2015). The Markov chain Monte Carlo (MCMC) chains were run for five million generations and ten independent runs. The state was sampled every 100 generations. Fixed JC + G (Jukes-Cantor + Gamma) were used for BBM analysis. The distribution range of all species of cricetids included in this work has been divided into eight geographic areas, which have been carefully chosen according to dissimilarities in their faunal composition that provided evidence for palaeobiogeographic or palaeoenvironmental differences between them. They correspond to: A (southwestern Europe), B (Central Europe), C (Greece), D (Anatolia-Caucasus), E (west central Asia), F (Arabian Peninsula), G (southern Asia) and H (east central Asia).

Biodiversity rates

The combination of cladistic and biodiversity analyses highlights the phenomena of speciation, extinction, and diversity changes in a given group over time (Stigall 2010, López-Antoñanzas et al. 2015). This allows establishing the timing of biodiversity crises and, thus, deducing possible causes.

Per-capita rates for speciation ($\hat{q}$), extinction ($\hat{p}$), and diversity change (d) have been calculated (Supplementary Tab. S2 available on Dryad) following the equations given by Foote (2000) according to which:

$$\hat{p} = -\mathrm{Ln}(Nbt/(Nbt + NFt))/\Delta t$$

$$\hat{q} = -\mathrm{Ln}(Nbt/(Nbt + NbL))/\Delta t$$

$$d = \hat{p} - \hat{q}$$

where Nbt indicates the number of species that cross both the upper and lower interval boundaries, NFt the number of species that originate within the interval and cross over the

upper interval boundary and NbL the number of species that cross the lower interval boundary, but become extinct during the interval and Δt the duration of the interval t_1-t_0.

Rates of biodiversity change (R), speciation (S), and extinction (E) have been calculated (Supplementary Tab. S2 available on Dryad) with the following equations (Stigall 2010):

$$R = (\ln N_1 - \ln N_0)/\Delta t$$

$$S = (\ln(N_0+o_0) - \ln N_0)/\Delta t$$

$$E = (\ln(N_0+o_0) - \ln N_1)/\Delta t$$

where N_0 is the initial number of species in a clade at time t_0, N_1 the number of species in a clade at time t_1, o_0 the number of speciation events during the interval t_1-t_0, and Δt the duration of the interval t_1-t_0.

All rates have been calculated each 0.5 Ma using the phylogenetically corrected species ranges obtained from the MCCT. Values calculated from the first and last intervals have been excluded from the analysis to remove edge effects, following the criterion of Stigall (2010).

RESULTS AND DISCUSSION

Tree Topology

Maximum Parsimony and tip-dated and undated Bayesian trees (Figs. 1, 2, Supplementary Figs.S2-S4 available on Dryad) show three large clades that correspond to the rodent subfamilies Megacricetodontinae, Democricetodontinae and Cricetodontinae. Both in, the majority consensus tree resulting from equal weights maximum parsimony and undated Bayesian analysis (Supplementary Figures S3 and S4 available on Dryad) show Megacricetodontinae and Cricetodontinae more closely related to one another than either one is to Democricetodontinae. However, some studies have evidenced that downweighting characters according to their homoplasy (applying implied weighting) improves morphological data sets, particularly those that are highly homoplastic, and produces more resolved and accurate trees than standard equal weights (Goloboff et al., 2008; Smith, 2019).

As a well-recognized problem when working on fossil rodents is the supposedly high homoplasy of dental characters, discussion on parsimony results will be based on the topology of the tree resulting from the implied weighting analysis.

Both implied weighting parsimony and tip-dated Bayesian analyses (Figs. 1 and 2) supported Cricetodontinae as the sister group to the clade consisting of Megacricetodontinae plus Democricetodontinae, which are sister clades of each other. These results place Democricetodontinae and Megacricetodontinae closer to one another than either is to the Cricetodontinae, which is in line with the phylogenetic hypothesis proposed by Flynn (2009).

Implied weights maximum parsimony—The topology of the tree shows three main clades: Megacricetodontinae, Democricetodontinae and Cricetodontinae.

The calibration of the strict consensus tree (Fig.1) shows that Democricetodontinae (node 83) originated circa 23.7 Ma. They share two non-exclusive synapomorphies (Supplementary Tab. S3, Supplementary Figure S1 (for numbers of each node in the tree) available on Dryad)), which are the presence of a double protoloph on M2 (29(0→1)) and the metacone absent or included in crest on M3 (50(0→2)). All the taxa included in this clade also share the exclusive synapomorphy of having an m1 with anteroconid in lingual position (60(0→1)).

Megacricetodontinae (node 138) originated approximately 23.7 Ma. They share three exclusive synapomorphies. The first one consists in having a divided anterocone with the lingual anterocone smaller than the labial one on M1 (5(0→2)). The second one rests in having m3 quite reduced (with an Lm1/Lm3 ratio between 1.4-1.6 mm) (67(0→2)) and the third one in having the entoconid small but still distinct on m3. The taxa included in this clade (except for *Megacricetodon andrewsi*) also share the non-exclusive synapomorphy of having M3 with usually incomplete central atoll (45(0→1)). Megacricetodontinae comprise two clades. The

first one regroups the species originating from node 137 (*Shamalina tuberculata* (*Punjabemys downsi*, *Sindemys shewanensis*)). It is supported by two non-exclusive synapomorphies: the presence of a small enterostyle isolated from the protocone and the lack of a well-developed anterolophid on m3 ((18(0→1); 73(0→1)). The second clade consists in all the species that originate from node 145 (*Aktaumys dzhungaricus* and more derived megacricetodontines). They share the non-exclusive synapomorphies of having on M1 the lingual anteroloph weak or absent (10(0→1)), a long mesoloph (19(1→0)) and the posteroloph that continues beyond the point where it meets the metalophule (23(0→1)), and in having the protoloph slightly anteriorly directed on M3 (41(0→1)).

Cricetodontinae are the species originating from node 91. They share the two exclusive synapomorphies of having the anterocone divided in two parts of similar size on M1 (5(0→1)) and a distinct anterior ectoloph (12(0→1)). They are also sustained by five non-exclusive synapomorphies: a long posteroloph that continues beyond the point where it meets the metalophule (23(0→1)), a large single anteroconid on m1 (54(0→1)) and the lingual anterolophid weak or absent on the lower molars (59(0→2), 68(0→1), 73(0→1)).

The split of Cricetodontinae from the sister clades Democricetodontinae plus Megacricetodontinae is set up circa 23.8 Ma. The basalmost taxa within Cricetodontinae are *Cricetodon versteegi* and, one node up, *C. goklerensis*, both from the Early Miocene of Turkey. The remaining taxa are split into two very asymmetrical branches. One is represented by plesiomorphic species of *Cricetodon* from the Early Miocene of Turkey (*C. fikreti* + *C. trallesensis*), whereas the other form a much larger group that includes all the remaining species of the subfamily. At the base of this clade a polytomy involving *Cricetodon fengi*,, *Mixocricetodon dehmi* plus *Cricetodon sonidensis*, and a clade comprising all the more derived species. The latter splits into two lineages. The smaller one includes the species originating from node 103 with *C. wanhei* as most basal and *C. aliveriensis* plus *C. kasapligili* as most

derived and *C. tobieni* in an intermediate position. This clade is supported by the non-exclusive and unambiguous synapomorphy of having a complete central atoll on M3 (a reversal). This character is only shared by the most plesiomorphic species of *Cricetodon* (*C. verstegi*) and most of *Democricetodon* spp. The larger branch is constituted by a succession of lineages, the most basal of which is that of the most plesiomorphic true European species, *C. meini* plus *C. aureus*. One node up *C. orientalis* from the Middle Miocene of China branches and then *C. soriae* from the Middle Miocene of Europe. The more derived species divide first in a clade of Middle Miocene European species of *Cricetodon* (*C. jotae*, *C. jumaensis*, *C. albanensis*, *C. bolliegeri*, *C. nievei*, *C. engesseri*). They share the two non-exclusive synapomorphies of having the lingual anteroloph of M2 poorly developed (26(0→1)) and M2 elongated (28(0→1)). The remaining species, originating from node 93, consist in a succession of European (*C. sansaniensis*, *C. hungaricus*, *C. caucasicus*) and Turkish (*C. pasalarensis*) taxa that splits (node 114) to give rise to *Byzantinia* and *Hispanomys* during the Middle Miocene. The bifurcation in which *Hispanomys* originated (node 113) includes the late Middle Miocene species of '*Cricetodon'* from Central Europe ('*C.*' *klariankae*, and '*C.*' *venczeli*), which should be considered as belonging to *Hispanomys*. Similarly, the bifurcation from which *Byzantinia* evolved (node 116) contains the Middle Miocene '*Cricetodon*' *fandli*, '*C.*' *candirensis* and '*C.*' *cariensis* basally, which may be reinterpreted, according to this analysis, as plesiomophic representatives of *Byzantinia*.

Tip-dated Bayesian analysis—The divergence between Cricetodontinae and Democricetodontinae + Megacricetodon is set up at approximately 28.2 Ma, and that between the sister clades Democricetodontinae and Megacricetodontinae circa 25.9 Ma.

Democricetodontinae: The topology of the tree (Fig. 2) shows two sister clades. The first includes two sister species: *Democricetodon sui* from the Early Miocene of China (21.9-21.16 Ma), which is the oldest record of *Democricetodon* in Asia (Maridet et al., 2011), and *Primus*

microps from the Early Miocene of Pakistan (circa 21-23 Ma) (Bruijn et al. 1981). The second one shows at the base the two plesiomorphic species of *Democricetodon* (*D. anatolicus* and *D. doukasi*) from the Early Miocene of Turkey, which insert sequentially on the steam, leading to more derived *Democricetodon* spp. *Democricetodon franconicus*, from the Early Miocene of Aliveri (Greece), is the most basal species of this clade. It is followed successively by *D. mutilus* and *D. gracilis*, which reveal the first entrance of Democricetodontinae in the central-western European bioprovince (circa 18.27 Ma). *D. gracilis* is sister species to a clade including mostly Asian species, providing evidence for an early Middle Miocene migration of *Democricetodon* from Europe towards China at approximately 16.1 Ma.

Megacricetodontinae: The topology of the tree (Fig. 2) shows two main clades within this subfamily of rodents. The first one includes an array of Early Miocene species of disputed origin (*Vallaris zappai*, (*Sindemys shewanensis*, *Punjabemys downsi*)). *Punjabemys downsi* from the Early Miocene of Pakistan was originally considered a member of Megacricetodontinae (Lindsay, 1988) and then as belonging to the Myocricetodontinae by Wessels (2009) together with *Vallaris zappai* and *Sindemys shewanensis* from the Early Miocene of Turkey and Pakistan, respectively. According to the topology of the tree, these taxa are either the basalmost representatives of Megacricetodontinae or could as well be considered as their sister group. Be that as it may, they are sister group to the clade that includes the other megacricetodontines, the basalmost taxon of which is *Shamalina tuberculata* from the Early Miocene of Saudi Arabia. This result agrees with Lindsay (1994), who thought that *Shamalina* could have given rise to *Megacricetodon*, but oppose the suggestion of Wessels (2009), who included this taxon within the Myocricetodontinae. *Shamalina* may have led to two main lineages. One consists of the sister species *Aktaumys dzhungaricus* and *Megacricetodon beijiangensis* and points to a dispersal event from Saudi Arabia towards Kazakhstan and China circa 21.28 Ma. The other lineage, which is more speciose, shows at its base *Megacricetodon*

hellenicus from the Early Miocene of Aliveri, Greece (Oliver and Peláez-Campomanes, 2014), which provides evidence for the first entrance of *Megacricetodon* into the Aegean-Anatolian region at approximately 19.5 Ma ago. One node further up two clades substantiates two independent migration events. One involved *Megacricetodon* aff. *collongensis* (circa 18 Ma), the most primitive species of the typical central European "*Megacricetodon bavaricus* group" proposed by Oliver and Peláez-Campomanes (2013), and the other *M. andrewsi* and *M. primitivus* at approximately 17 Ma. These results agree with Oliver and Peláez-Campomanes (2016), who inferred at least three migration events in Europe for early *Megacricetodon* forms on the basis of important morphological differences.

Cricetodontinae originated in Turkey at approximately 25 Ma (Fig. 2). The basalmost taxon is *C. versteegi* and *C. goklerensis* is one node up in the clade. Both taxa come from the lower Miocene of Turkey (de Bruijn et al. 1993; Joniak et al. 2017). *Cricetodon goklerensis* is sister species to a large group that includes all the remaining species of the subfamily, the basalmost clade of which includes the most plesiomorphic species of *Cricetodon*, mostly from Turkey and China, and documents the first entrance of *Cricetodon* from Turkey into China at *circa* 19.4 Ma. The split of this basal clade and the clade comprising more derived species of Cricetodontinae is set up at 22.3 Ma. Within the latter, the most basal taxa are represented by the Turkish Early Miocene species *C. fikreti* and *C. trallesensis*. *Cricetodon trallesensis* diverges from the main clade approximately 20 Ma ago and led to two clades. The first one includes practically all European Middle Miocene species of *Cricetodon* and reveals the first entrance of the Cricetodontinae into Europe circa 17.77 Ma. The presence inside this group of the Asiatic species *C. orientalis* provides evidence for a second dispersal of Cricetodontinae into China, this time from Europe, which took place approximately 16.8 Ma. The second clade comprises the most derived species of Cricetodontinae. A sequence of the three most basal taxa from the Middle Miocene of Central Europe and Turkey (*C. hungaricus*, *C. caucasicus*, *C.*

pasalarensis) insert sequentially on the steam, leading to two important lineages. One leads to *Hispanomys* and includes the late Middle Miocene species of "*Cricetodon*" from Central Europe (*C. fandli*, *C. klariankae* and *C. venzecli*), which should be considered to belong to *Hispanomys,* according to this analysis. Similarly, the bifurcation from which *Byzantinia* evolved contains, in a basal position, the Middle Miocene *Cricetodon cariensis* and *C. candirensis*, which would be plesiomophic representatives of *Byzantinia*.

Bayesian analyses versus Parsimony

Tree topologies of undated Bayesian and equal weights maximum parsimony searches are more similar to each other than either is to the implied weighting parsimony and tip-dating Bayesian trees. In the same way, the topologies of implied weighting parsimony and tip-dating Bayesian trees are more similar to each other than either to the two other topologies. Despite the fact that the topologies of implied weight parsimony and tip-dated Bayesian trees (Figs. 1, 2) are similar as far as the relationships between large clades are concerned, they differ in the placement of some taxa amongst the lineages inside these clades. This issue holds particularly true for the clades that are not comprehensively sampled (e.g., Democricetodontinae and Megacricetodontinae vs Cricetodontinae) and those that are weakly supported. Because of the differences recovered between the topologies resulting from different methods, stratigraphic congruence indices have been calculated to assess how well each of these phylogenies fits with the chronostratigraphy. Our results show high levels of stratigraphic congruence for all metrics for parsimony (equally weights and implied weights) and both Bayesian (undated and tip-dating) methods (Supplementary Tab. S4 available on Dryad). As expected, the maximum credibility tree recovered by tip-dating has significantly higher stratigraphic congruence than the majority consensus trees resulting from undated Bayesian and parsimony analyses (Supplementary Tab. S4 available on Dryad). The majority consensus tree resulting from implied weighting parsimony (similar to the strict consensus tree) has higher stratigraphic

405 congruence than the majority consensus trees recovered from equal weights parsimony and
406 undated Bayesian searches. Recent studies provided evidence that the inclusion of stratigraphic
407 age data in tip-dating impacts the topology of the tree, particularly when the datasets include
408 incompletely scored taxa or taxa having weak character support (King 2021). The differences
409 we found between the topologies of the tip-dated Bayesian tree and the undated Bayesian and
410 parsimony trees are probably due to the presence of highly homoplastic characters in our
411 dataset. Taken into account that the topology of the undated phylogenies shows some
412 anomalous results (e.g. derived position of the oldest democricetodontines) and that time-
413 scaling these topologies (Fig. 1) results in improbable long ghost lineages for a large number
414 taxa, we consider that the topology obtained via the tip-dating Bayesian analyses is most likely
415 to be more accurate with our kind of morphological dataset (fossil rodent teeth). Therefore, the
416 discussion on palaeogeography and biodiversity will be based on the Maximum Clade
417 Credibility Tree (MCCT) resulting from the tip-dating Bayesian analysis (Fig. 2). Interestingly,
418 Lee and Yates (2018) also found that tip-dating approaches were better able to elucidate the
419 relationship of some crocodilian groups that showed extensive convergent adaptations.
420
421 *Palaeobiogeographic framework*

422 During the Miocene, Democricetodontinae, Megacricetodontinae and Cricetodontinae were
423 successful and exhibited a wide distribution, ranging geographically from western Europe to
424 eastern Asia. Their evolution is complex and involves indigenous speciation phenomena and
425 numerous intercontinental dispersal events. According to our results most immigration events
426 involved Turkey (Fig. 3). Democricetodontinae may have originated in Turkey approximately
427 24.8 Ma and entered Asia about 23.9 Ma. The results of this work also provides evidence of a
428 probable Turkish origin for European Democricetodontinae with a first arrival in central and
429 western Europe circa 18.3 Ma. The delayed entrance of this group into Europe was probably

due to the geographical isolation of the Dinarian-Anatolian Island (Neubauer et al. 2015). A Middle Miocene dispersal of *Democricetodon* from Europe to China has been evidenced in this work and set up around 16.1 Ma.

A more comprehensive phylogenetic analysis that includes the Myocricetodontinae is needed to elucidate if *Vallaris zappai* and more derived taxa belong to the Megacricetodontinae or are, actually, closer to the Myocricetodontinae. Without this information, two scenarios are plausible. The first one points to a Turkish origin of Megacricetodontinae circa 23.3 Ma, whereas in the second one they would originate from either Turkey or Saudi Arabia around 22.6 Ma. The eastwards dispersal to Kazakhstan and western China is set circa 21.3 Ma and that to the Aegean-Anatolian area (where they are recorded in Aliveri and Këwhile sekoy) circa 19.5 Ma. Two independent dispersal events took place then from this area towards the West first and then toward eastern China, and Central Europe at approximately 18 Ma. A subsequent dispersal from western Asia to the Aegean-Anatolian area occurred approximately one million years later (circa 17 Ma) (Fig. 3).

Cricetodontinae are supposed to have originated from Turkey at 25 Ma, where several lineages differentiated, and then passed into Greece at the earliest at 20 Ma and to eastern Asia around 19.4 Ma (Fig. 3). Greek cricetodontines from the Early Miocene of Aliveri are not closely related to the European Middle Miocene cricetodontines but to the Turkish Early Miocene ones. In fact, at this time, Aliveri may not have belonged to the European region but to the Aegean-Anatolian one, which was only intermittently in contact with Europe. Most of the European cricetodontines originated from an independent Turkish lineage that dispersed into the south-western part of the continent circa 18.5 Ma. Two dispersal events towards central Europe occurred at 16.4 Ma and 15.5 Ma and two additional ones towards the Aegean-Anatolian area and western China are inferred at 16.8 Ma and 16.2 Ma. On the basis of our analysis, it turns out that the Late Miocene cricetodontines are not closely related to the Middle

Miocene European ones. In fact, one important dispersal event at about 16.4 Ma from Turkey towards Europe together with an independent evolution in Turkey led to a later development of two dynamic centres of speciation in southwestern and central Europe (*Hispanomys*) and Anatolia (*Byzantinia*).

Palaeoclimatic context

During the Oligocene and the Early Miocene, the East Antarctic Ice Sheet was relatively unstable with periods of growth and others of decline (Miller et al., 2020). At the Eocene/Oligocene Transition and the beginning of the Oligocene (33.9-32 Ma), a large deglaciation triggered successive sea level rises up to 50 m. On the contrary, sea-level drops were recorded in early Late Oligocene times, at approximately 28 Ma (Oi1), and at the beginning of the Miocene, circa 23 Ma (Mi1) (Miller et al., 2020). Interestingly, this sea-level fall at the Oligocene/Miocene boundary coincides with a severe restriction of the marine connections between the Indian Ocean and the Mediterranean Sea (Hüsing et al., 2009). This could have opened dispersal land routes that could have allowed the migration of primitive megacricetodontines, such as *Shamalina tuberculata* from Saudi Arabia towards Kazakhstan and western China (~23.5 Ma). The dispersal of *Democricetodon* from Turkey to Pakistan and China (~23.9 Ma) might have been elicited by the same phenomenon. Until the beginning of the Miocene Climatic Optimum (17-15 Ma), eustatic sea level changes indicates the presence of a moderate to large ice sheet in Antarctica (Miller et al. 2020). Low sea level that allowed dispersal of faunas are indicators of cool intervals, whereas higher sea levels represents warmer periods. Climate variations are expected to have played a major role in shaping the diversity of small mammals in general and rodents in particular. So, confronting the timing of shifts of diversification and climatic perturbations can provide lines of evidence regarding the influence of the latter on the former. The analysis of the shifts of diversification across the phylogeny of Cricetodontinae, the most comprehensive subclade in this work, is shown in Fig. 4.

Regrettably, the poor fossil record of Cricetodontinae in Turkey between 23 Ma and 19 Ma, where and when this group originated and started diversifying, does not allow a robust interpretation of our results during this interval of time. The MCO (~17-15 Ma) was a warm period that is mostly characterized by high sea level and reduced ice volume. Since a little before the Miocene Climatic Optimum (18.5 Ma) and nearly throughout all of it, the rodent community of cricetodontines experienced a period of stability and success, during which the biodiversity was slightly but constantly increasing (Fig. 4). This increase in biodiversity resulted from a continuous decrease in the extinction rate of these rodents together with high speciation rates that remained nearly constant. At approximately 16.0 Ma, an interruption of the Miocene Climatic Optimum is evinced by a sea level fall of ~40 m (Mi2) (Miller et al. 2020), which would have allowed the second dispersal of *Democricetodon* from westwards to eastwards. This cooling event (Mi2) seems to have promoted a drop in the speciation of Middle Miocene European cricetodontines, which was fairly high up to that point (Fig. 4), while their extinction rate continued to decrease. After the MCO and during the Middle Miocene Climatic Transition (~15-13 Ma), three events of cooling and sea-level fall at 14.8 (Mi2a), 13.8 (Mi3) and 12.8 Ma (Mi4) took place that culminated with the establishment of the "permanent East Antartic Ice Sheet" (Miller et al. 2020). After the Mi2 event, speciation and extinction rates tended to decrease continuously. However, our results show high extinction and speciation rates that are coupled with the Miocene cooling events Mi3 and Mi4 (Fig. 4). The most prominent turnover is detected during the Mi3 event (circa 13.8 Ma). Interestingly, this event seems to have been particularly impactful in southern Europe, where most of the cricetodontines lived at this time. Actually, a sudden and important drop in temperatures was evidenced in Spain after analysing oxygen isotopes of mammal teeth enamel (Domingo et al. 2009, 2012). The evolutionary radiation of various endemic lineages of *Byzantinia*, in Anatolia, and *Hispanomys*, in Europe, took place during the Mi3 event (Fig. 4). In these areas, parallel lineages showed similar trends towards an increase of size, a reduction of length of the

506 third molars and the development of a complete backwards paracone spur (Rummel 1998).
507 This suggests a specialisation toward food that includes more abrasive and fibrous plants,
508 indicating in turn increasingly open environments. When *Byzantinia* and *Hispanomys*
509 flourished, their potential competitors such as the Middle Miocene cricetodontines were driven
510 to extinction. At the beginning of the Late Miocene, at about 11.5 Ma (Mi5), another cooling
511 event associated with an increase in the ice volume in Antarctica took place (Cook et al., 2008).
512 This event is linked to a faunal turnover within the Cricetodontinae in which a drop in
513 biodiversity caused by elevated extinction rates (oldest taxa belonging to *Byzantinia*) was
514 followed by a second radiation of the most derived species of *Hispanomys* and *Byzantinia*.

515 It is evident that climatic events impacted the evolutionary history of the Cricetodontines.
516 However, given that some of the oldest taxa belonging to *Byzantinia* are not dated precisely,
517 the high extinction and speciation rates that we found in Mi5 may be exaggerated, whereas
518 those corresponding to Mi 4 might be minored.
519

520 CONCLUSION

521 Our analyses evidence that time-calibrated Bayesian searches yield trees that have higher
522 stratigraphic congruence compared with trees from undated Bayesian and parsimony
523 searches. Majority and strict consensus trees resulting from implied weights parsimony show
524 the second best stratigraphic concordance values. They are followed by equal character
525 weighting parsimony and non-clock Bayesian searches. So, according to our results, if
526 stratigraphic congruence is taken as a proxy for phylogenetic accuracy, then time-calibrated
527 Bayesian inference analysis (morphological clock) is probably the more accurate method for
528 analysing morphological characters with a high degree of homoplasy (such as those of rodent
529 teeth). However, more studies comparing morphological parsimony and time-calibrated and
530 not time-calibrated Bayesian methods are needed to conclude which of these approaches deal

better with the morphological characters provided by fossil rodents, which are mainly based on the dentition and considered highly convergent.

The Miocene is marked by obvious manifestations of climatic changes, which turn out to have been very influential in the evolution of animal life. Cricetids arrived at different times in different areas around the Mediterranean and became extinct asynchronously as well. Our results suggest that the Miocene cooling events, particularly Mi2, Mi3, Mi4 and Mi5 that took place at 16 Ma, 13.8 Ma, 12.8 Ma and 11.5, respectively, impacted cricetid evolution by promoting dispersal and triggering important origination/extinction events.

DATA AVAILABILITY

The data underlying this article are available in the article and from the Dryad Digital Repository https://datadryad.org/stash/share/Dmda4GGW64PE8-c4fZiwP2VpbnTlTZpWm4PRSm5L20Q

ACKNOWLEDGMENTS

We sincerely thank the instructors T. Simões (Harvard University, Cambridge, USA) and O. Vernygora (University of Kentucky, Lexington, USA) of the Transmitting Science Course "Morphological Phylogenetics" for kindly answering our inquiries. Further thanks for helpful comments and constructive criticism are given to O. Vernygora, who also reviewed this article together with two anonymous reviewers as well as the associate editor A. Wright (Southeastern Louisiana University, Hammond, USA).

FUNDING

This research received support from the research project PGC2018-094122-B-100 (MICU/AEI/FEDER,EU) and the SYNTHESYS+ project (http://www.synthesys.info), which is financed by European Commission.

557 REFERENCES

558 Bapst D.W. 2012. paleotree: an R package for paleontological and phylogenetic analyses of
559 evolution. Methods Ecol. Evol. 3:803–807.

560 Bapst D.W. 2014. Assessing the effect of time-scaling methods on phylogeny-based analyses
561 in the fossil record. Paleobiology.40:331–351.

562 Barido-Sottani J., Aguirre-Fernández G., Hopkins M.J., Stadler T., Warnock R. 2019.
563 Ignoring stratigraphic age uncertainty leads to erroneous estimates of species divergence
564 times under the fossilized birth–death process. Proc. R. Soc. B. 286:2019068520190685

565 Bell M.A. and Lloyd G.T. 2014 strap: An R package for plotting phylogenies against
566 stratigraphy and assessing their stratigraphic congruence. Palaeontology. 58:379–389.

567 Benton M.J., Storrs G.W. 1994. Testing the quality of the fossil record: paleontological
568 knowledge is improving. Geology. 22:111–114.

569 Benton MJ. 2015 Exploring macroevolution using modern and fossil data. Proc. R. Soc. B.
570 282:20150569.

571 Bouckaert R., Heled J., Kühnert D., Vaughan T., Wu C.H., Xie D., Suchard M.A., Rambaut
572 A., Drummond A.J. 2014. BEAST 2: A Software Platform for Bayesian Evolutionary
573 Analysis. PLoS Computational Biology. 10:e1003537.

574 Bremer K. 1994. Branch support and tree stability. Cladistics. 10:295–304.

575 Casanovas-Vilar I, Garcés M. Van Dam J., García-Paredes I., Robles J.M., Alba D.M. 2016.
576 An updated biostratigraphy for the late Aragonian and Vallesian of the Vallès-Penedès
577 Basin (Catalonia, Spain). Geol. Acta 14:195-217.

578 Cooke P.J., Nelson C.S., Crundwell M.P. 2008. Miocene isotope zones, paleotemperatures,
579 and carbon maxima events at intermediate water-depth, Site 593, Southwest Pacific, New
580 Zealand. J. Geol. Geophys. 51:1–22.

581 Daams R., Freudenthal M. 1989. Cricetidae (Rodentia) from the type-Aragonian; the genus
582 *Megacricetodon*. Scr. Geol. 1:39–132.

583 De Bruijn, H. 1976. Vallesian and Turolian rodents from Biotia, Attica and Rhodes (Greece).
584 Proc. Kon. Nederl. Akad. Wetensch. B. 79:361–384.
585 De Bruijn H., Hussain S.T., Leinders, J.M. 1981. Fossil rodents from the Murree formation
586 near Banda Daud Shah, Kohat, Pakistan. Proc. Kon. Nederl. Akad. Wetensch. B. 84:71–
587 99.
588 De Bruijn H., Fahlbusch V., Saraç G., Ünay E. 1993. Early Miocene rodent faunas from the
589 eastern Mediterranean areas. III: the genera Deperetomys and Cricetodon with a
590 discussion of the evolutionary history of the Cricetodontini. Proc. Kon. Nederl. Akad.
591 Wetensch. B. 96:151–216.
592 Domingo L., Cuevas González J., Stephen T.G., Hernández Fernández M., López-Martínez
593 N., 2009. Multiproxy reconstruction of the palaeoclimate and palaeoenvironment of the
594 Middle Miocene Somosaguas site (Madrid, Spain) using herbivore dental enamel.
595 Palaeogeogr. Palaeoclimatol. Palaeoecol. 272:53–68.
596 Domingo L., Koch P.L., Grimes S.T., Morales J., López-Martínez N., 2012. Isotopic
597 paleoecology of mammals and the Middle Miocene Cooling event in the Madrid Basin
598 (Spain). Palaeogeogr. Palaeoclimatol. Palaeoecol. 339:98–113.
599 Fisher D.C. 1994. Stratocladistics: morphological and temporal patterns and their relation to
600 phylogenetic process. In: Grand L., Rieppel O., editors. Interpreting the hierarchy of
601 nature. San Diego: Academic Press, p. 133–171.
602 Flynn L.J. 2009. The antiquity of *Rhizomys* and independent acquisition of fossorial traits in
603 subterranean muroids. Bull. Am. Mus. Nat. Hist. 331:128–156.
604 Flynn L.J., Pilbeam D., Barry J.C., Morgan M.E., Raza S.M. 2016. Siwalik synopsis: A long
605 stratigraphic sequence for the Later Cenozoic of South Asia. C. R. Palevol. 15:877–887.
606 Foot M. 2000. Origination and extinction components of taxonomic diversity: general
607 problems. Paleobiol. 26: 74–102.

608 Goloboff P.A., Farris J.S. 2001. Methods for quick consensus estimation. Cladistics. 17:26–
609 34.
610 Goloboff P.A. 1999. Analyzing large data sets in reasonable times: solutions for composite
611 optima. Cladistics.15:415–428.
612 Goloboff P.A., Farris J.S., Nixon K.C. 2003. TNT: Tree Analysis Using New Technology.
613 Program and documentation, available from the authors at www.lillo.org.ar/phylogeny/tnt/
614 Goloboff P.A., Carpenter J.M., Arias J.S., Esquivel D.R.M. 2008. Weighting against
615 homoplasy improves phylogenetic analysis of morphological data sets. Cladistics. 24:758–
616 773.
617 Goloboff P.A., Farris J.S., Nixon K.C. 2008. TNT, a free program for phylogenetic analysis.
618 Cladistics. 24: 774–786.
619 Goloboff P.A., Torres A., Arias J.S. 2017. Weighted parsimony outperforms other methods of
620 phylogenetic inference under models appropriate for morphology. Cladistics. 34:407–437.
621 Heath T.A., Huelsenbeck J.P., Stadler T. 2014. Fossilized birth–death process. PNAS.
622 111:E2957–E2966.
623 Hír J., Venczel M., Codrea V., Angelone C., van den Hoek Ostende L.W., Kirscher U., Prieto
624 J. 2016. Badenian and Sarmatian s.str. from the Carpathian area: Overview and ongoing
625 research on Hungarian and Romanian small vertebrate evolution. C. R. Palevol. 15:863–
626 875.
627 Huelsenbeck J.P. 1994 Comparing the stratigraphic record to estimates of phylogeny.
628 Paleobiology. 20:470–483.
629 Hüsing S.K., Zachariasse W.J., van Hinsbergen D.J.J., Murat Inceöz, W. K., Harzhauser M.,
630 Mandic O., Krohet A. 2009. Oligocene–Miocene basin evolution in SE Anatolia, Turkey:
631 constraints on the closure of the eastern Tethys gateway. Geol. Soc. London. Spec. Publ.
632 311:107–132.

633 Hunt G., Slater G. 2016. Integrating Paleontological and Phylogenetic Approaches to
634 Macroevolution. Annu. Rev. Ecol. Evol. Syst. 47:189−213.
635 Joniak P., De Bruijn H. 2014. Rodents from the Upper Miocene Tuğlu Formation (Çankiri
636 Basin, Central Anatolia, Turkey). Palaontol Z. 89:1039–1056.
637 Joniak P., Peláez-Campomanes P., van den Hoek Ostende L.W., Rojay B. 2017. Early
638 Miocene rodents of Gökler (Kazan Basin, Central Anatolia, Turkey), Hist. Biol. 31:982–
639 1007.
640 King B. 2021. Bayesian tip-dated phylogenetics in paleontology: topological effects and
641 stratigraphic fit. Syst. Biol. 70:283–294.
642 King B., Beck R. 2019. Bayesian Tip-dated Phylogenetics: Topological Effects, Stratigraphic
643 Fit and the Early Evolution of Mammals. bioRxiv 533885.
644 Lee M.S., Palci A. 2015. Morphological Phylogenetics in the Genomic Age. Curr. Biol.
645 25:R922−9.
646 Lee M.S.Y., Yates A.M. 2018. Tip-dating and homoplasy: reconciling the shallow molecular
647 divergences of modern gharials with their long fossil record. Proc. R. Soc. B 285:
648 20181071.
649 Lewis P.O. 2001. A likelihood approach to estimating phylogeny from discrete
650 morphological character data. Syst. Biol. 50:913–925.
651 Lindsay E.H. 1988. Cricetid rodents from Siwalik deposits near Chinji Village, part 1:
652 Megacricetodontinae, Myocridetontinae and Dendromurinae. Paleovertebrara 18:95–154.
653 Lindsay E.H. 1994. Fossil record of Asian Cricetidae with emphasis on Siwalik cricetids. In:
654 Tomida Y., Li C.K., Setoguchi T., editors. Rodent and Lagomorph Families of Asian
655 Origins and Diversification. National Science Museum Monographs, 8. p. 131–147.
656 Lindsay E.H. 2017. *Democricetodon fejfari* sp. nov. and replacement of Cricetidae by
657 Muridae in Siwalik deposits of Pakistan. Foss. Impr. 73:445–453.

López-Antoñanzas R., Knoll F., Wan S., Flynn L.J. 2015. Causal evidence between monsoon and evolution of rhizomyine rodents. Sci. Rep. 5:9008.

Maddison W.P., Maddison D.R., 2009. Mesquite: A Modular System for Evolutionary Analysis, ver. 2.6. Mesquite Project, Vancouver.

Maridet O., Wu W.Y, Ye J., Bi S.D., Ni X., Meng J. 2011. Early Miocene cricetids (Rodentia) from the Junggar basin (Xinjiang, China) and their biochronological implications. Geobios. 44: 445–459.

Miller K.G., Browning J.V., Schmelz W.J., Kopp R.E., Mountain G.S., Wright J.D. 2020. Cenozoic sea-level and cryospheric evolution from deep-sea geochemical and continental margin records. Sci. Adv. 6:eaaz1346.

Miller M.A., Pfeiffer W., Schwartz T. 2010. Creating the CIPRES Science Gateway for inference of large phylogenetic trees. In: 2010 gateway computing environments workshop. p. 1–8.

Mitchell J., Etienne R.S., Rabosky D.L. 2019. Inferring diversification rate variation from phylogenies with fossils. Syst. Biol. 68:1–18.

Norell M.A., Novacek M.J. 1992. Congruence between superpositional and phylogenetic patterns: comparing cladistic patterns with fossil records. Cladistics. 8:319–337.

Norell M.A., Novacek M.J., Wheeler Q.D. 1992. Taxic origin and temporal diversity: the effect of phylogeny. In: Novacek M.J., Wheeler Q.D., editors). Extinction and phylogeny. Columbia University Press, p. 89–118.

O'Connor A. and Wills M.A. 2016. Measuring stratigraphic congruence across Trees, higher taxa, and time. Syst Biol. 65:792–811.

Oliver A., Peláez-Campomanes P. 2014. Evolutionary patterns of early and middle Aragonian (Miocene) of *Megacricetodon* (Rodentia, Mammalia) from Spain. Palaeontographica. A. 303:85–135.

Pol D. 2001 Comments on the Manhattan stratigraphic measure. Cladistics 17, 285–289.

684 problems. Paleobiology. 26:74–102.
685 Prieto J., Rummel M. 2016. Some consideration on small mammal evolution in
686 SouthernGermany, with emphasis on Late Burdigalian-Earliest Tortonian (Miocene)
687 cricetid rodents. C. R. Palevol. 15:837–854.
688 Qiu Z., Li Q. 2016. Neogene rodents from central Nei Mongol, China. Palaeontol. Sinica N.
689 Ser. C. 198:1–684.
690 Reichenbacher B., Krijgsman W., Lataster Y. Pippèrr M., Van Baak C.G.C., Chang, L.,
691 Kälin, D., Jost J., Doppler, G. , Jung, D., Prieto, J., Aziz, H.A., Böhme, M. Garnish,
692 J.,Kirscher U, Bachtadse, V. 2013. A new magnetostratigraphic framework for the Lower
693 Miocene (Burdigalian/Ottnangian, Karpatian) in the North Alpine Foreland Basin. Swiss.
694 J. Geosci. 106:309–334.
695 Ronquist F, Teslenko M, van der Mark P, Ayres DL, Darling A, Höhna S, Larget B, Liu L,
696 Suchard MA, Huelsenbeck JP. 2012. MrBayes 3.2: efficient Bayesian phylogenetic
697 inference and model choice across a large model space. Syst. Biol. 61:539–542.
698 Ronquist F., Lartillot N., Phillips M.J. 2016. Closing the gap between rocks and clocks using
699 total-evidence dating. Phil. Trans. R. Soc. B. 371:20150136.
700 Rummel M. 1998. Die Cricetiden aus dem Mittel- und Obermiozän der Türkei. Doc. Naturae.
701 123:1–300.
702 Sansom R.S., Choate P.G., Keating J.N., Randle E. 2018. Parsimony, not Bayesian analysis,
703 recovers more stratigraphically congruent phylogenetic trees. Biol. Lett. 14:20180263.
704 Simões T.R., Caldwell M.W., Tałanda M., Bernardi M., Palci A., Vernygora O., Bernardini
705 F., Mancini L., Nydam, R.L. 2018. The origin of squamates revealed by a Middle Triassic
706 lizard from the Italian Alps. Nature. 557:706–709.
707 Simões T.R., Vernygora O., Caldwell M.W., Pierce S.E. 2020a. Megaevolutionary dynamics
708 and the timing of evolutionary innovation in reptiles. Nat. Commun. 11:3322.
709 Simões T.R., Caldwell M.W., Pierce S.E. 2020b. Sphenodontian phylogeny and the impact

710 of model choice in Bayesian morphological clock estimates of divergence times and
711 evolutionary rates. BMC Biology.18:191.
712 Stadler T. 2010. Sampling-through-time in birth–death trees. J. Theor. Biol. 267:396–404.
713 Stehlin H.G. 1910. Remarques sur les faunules de Mammifères des couches éocènes et
714 oligocènes du Bassin de Paris. Bull. Soc. Géol. France. 4:488–520.
715 Stigall-Rode A.L., Lieberman B.S. 2005. Using environmental niche modeling to study the
716 Late Devonian biodiversity crisis. In: Over D.J., Morrow J.R., Wignall P.B., editors.
717 Understanding Late Devonian and Permian-Triassic Biotic and Climatic Events: Towards
718 an Integrated Approach. New York, NY: Elsevier. p. 93–179.
719 Stigall A.L. 2010. Invasive species and biodiversity crises: Testing the link in the Late
720 Devonian. PLoS One. 5:e15584.
721 Tong Y.S. 1992. *Pappocricetodon*, a pre-Oligocene cricetid genus (Rodentia) form Central
722 China. Vertebrata PalAsiatica 30:1–16.
723 Ünay E., de Bruijn H., Saraç, G. 2003. A preliminary zonation of the continental Neogene of
724 Anatolia based on rodents. Deinsea, 10:539–547.
725 Van der Meulen A., García-Paredes I., Alvarez-Sierra M.A, van den Hoek Ostende L.W.,
726 Hordijk K., Oliver A., Pelaez-Campomanes P. 2012. Updated Aragonian biostratigraphy:
727 Small Mammal distribution and its implications for the Miocene European Chronology.
728 Geol. Acta. 10:159–179.
729 Varela L., Tambusso, P.S., McDonald, H.G., Fariña, R.A. 2019. Phylogeny,
730 macroevolutionary trends and historical biogeography of sloths: insights from a Bayesian
731 morphological clock analysis. Syst. Biol. 68:204–218.
732 Wagner P.J. 1995. Stratigraphic tests of cladistic hypotheses. Paleobiol. 21:153–178.
733 Wang X., Flynn L.J., Fortelius, M., editors. 2013. Fossil Mammals of Asia: Neogene
734 Biostratigraphy and Chronology. New York, Columbia University Press.

735 Wessels W. 2009. Miocene rodent evolution and migration: Muroidea from Pakistan, Turkey
736 and Northern Africa. Geol. Ultraiectina. 307:1–290.
737 Whybrow P.J., Collison M. E., Daams R., Gentry A.W., McClure H.A. 1982. Geology, fauna
738 (Bovidae, Rodentia) and flora from the early Miocene of eastern Saudi Arabia. Ter.
739 Research. 4:105–120.
740 Wills M.A. 1999 Congruence between phylogeny and stratigraphy: randomization tests and
741 the gap excess ratio. Syst. Biol. 48:559–580.
742 Wills M.A., Barret P.M, Heathcote J.F. 2008. The modified Gap Excess Ratio (GER*) and
743 the stratigraphic congruence of dinosaur phylogenies. Syst. Biol. 57:891–904.
744 Wright D.F. 2017. Bayesian estimation of fossil phylogenies and the evolution of early to
745 middle Paleozoic crinoids (Echinodermata). J. Paleontol. 91:799−814.
746 Wright A.M., Lloyd, G.T. 2020. Bayesian analyses in phylogenetic palaeontology:
747 interpreting the posterior sample. Palaeontology 63:997-1006.
748 Yu Y., Harris A.J., Blair C. and Xingjin H. 2015. RASP (Reconstruct Ancestral State in
749 Phylogenies): A tool for historical biogeography. Mol. Phylogenetics Evol. 87:46–49.

750

751 **Figure 1.** Calibrated strict consensus tree of cricetid rodents and their recorded temporal ranges
752 (black). Dashed bars indicate age uncertainty. Grey bars represent missing ranges and missing
753 ancestral lineages. Biochronological data from Casanovas et al. 2016; de Bruijn 1976; Flynn
754 2016; Hir et al. 2016; Joniak and de Bruijn 2014; Joniak et al. 2017; Lindsay 2017; Prieto and
755 Rummel 2016; Reichenbacher et al. 2013; Qiu and Li 2016; Ünay et al. 2003; Van der Meulen
756 et al. 2012; Wang et al., 2013; Wessels 2009; Whybrow et al. 1982.

757

758 **Figure 2.** Time-calibrated relaxed-clock Bayesian inference analysis with morphological tip-
759 dating using the fossilized birth–death tree model. Summary of the MCCT depicting the
760 median divergence time estimates for different cricetid lineages against a geological time
761 scale. Numbers at nodes indicate median estimates for the divergence times, and node bars
762 indicate the 95% highest posterior density for divergence times.

763

764 **Figure 3.** Ancestral state distributions at each node of the MCCT of cricetid obtained by BBM
765 analysis implemented in RASP against a geological time scale. Pie charts indicate probabilities
766 of alternative ancestral ranges. The colour indicates possible ancestral ranges at different nodes.
767 The schematic map shows the biogeographical areas used in this work and colours correspond
768 to: ocher (southwestern Europe), purple (central Europe), dark red (Greece), orange (Anatolia-
769 Caucasus), green (west central Asia), light blue (Arabian Peninsula), dark blue (southern Asia)
770 and yellow (east-central Asia).

771

772 **Figure 4.** Instantaneous per-capita (top) and deterministic (bottom) rates for Cricetodontinae
773 speciation ($\hat{p}$, S), extinction ($\hat{q}$, E), and biodiversity change (d, R) calculated using

774 phylogenetically constrained species ranges. Miocene cooling events against geological time

775 are indicated as Mi.

776

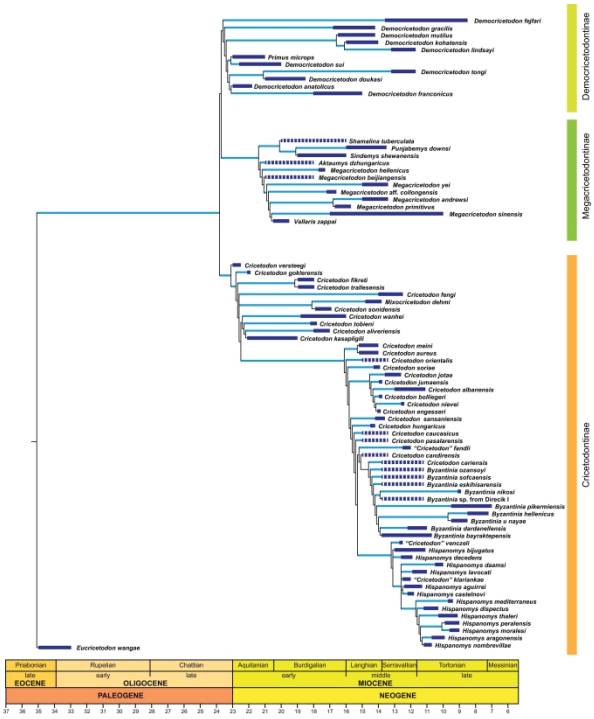

Figure 1. Calibrated strict consensus tree of cricetid rodents and their recorded temporal ranges (black). Dashed bars indicate age uncertainty. Grey bars represent missing ranges and missing ancestral lineages. Biochronological data from Casanovas et al. 2016; de Bruijn 1976; Flynn 2016; Hir et al. 2016; Joniak and de Bruijn 2014; Joniak et al. 2017; Lindsay 2017; Prieto and Rummel 2016; Reichenbacher et al. 2013; Qiu and Li 2016; Ünay et al. 2003; Van der Meulen et al. 2012; Wang et al., 2013; Wessels 2009; Whybrow et al. 1982.

432x307mm (300 x 300 DPI)

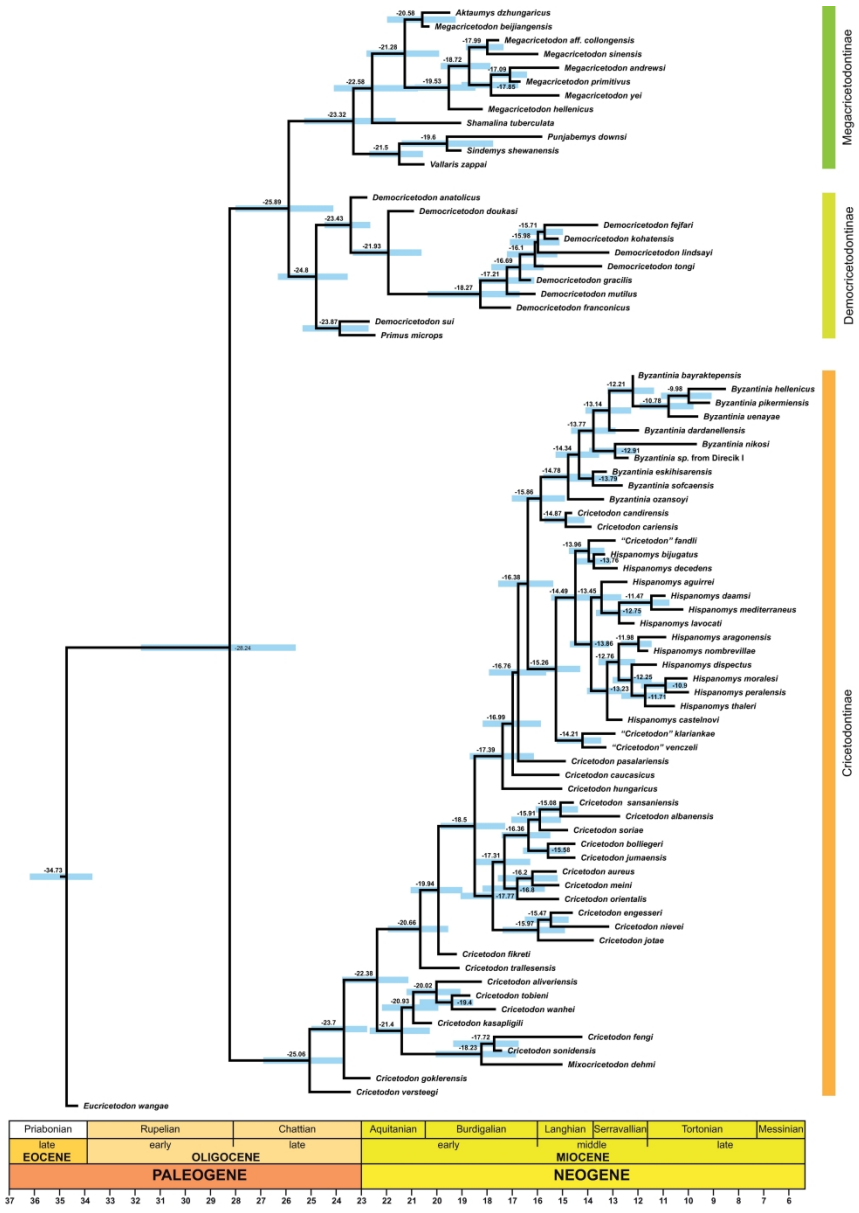

Figure 2. Time-calibrated relaxed-clock Bayesian inference analysis with morphological tip-dating using the fossilized birth–death tree model. Summary of the MCCT depicting the median divergence time estimates for different cricetid lineages against a geological time scale. Numbers at nodes indicate median estimates for the divergence times, and node bars indicate the 95% highest posterior density for divergence times.

274x385mm (300 x 300 DPI)

Figure 3. Ancestral state distributions at each node of the MCCT of cricetid obtained by BBM analysis implemented in RASP against a geological time scale. Pie charts indicate probabilities of alternative ancestral ranges. The colour indicates possible ancestral ranges at different nodes. The schematic map shows the biogeographical areas used in this work and colours correspond to: ocher (southwestern Europe), purple (central Europe), dark red (Greece), orange (Anatolia-Caucasus), green (west central Asia), light blue (Arabian Peninsula), dark blue (southern Asia) and yellow (east-central Asia).

168x409mm (300 x 300 DPI)

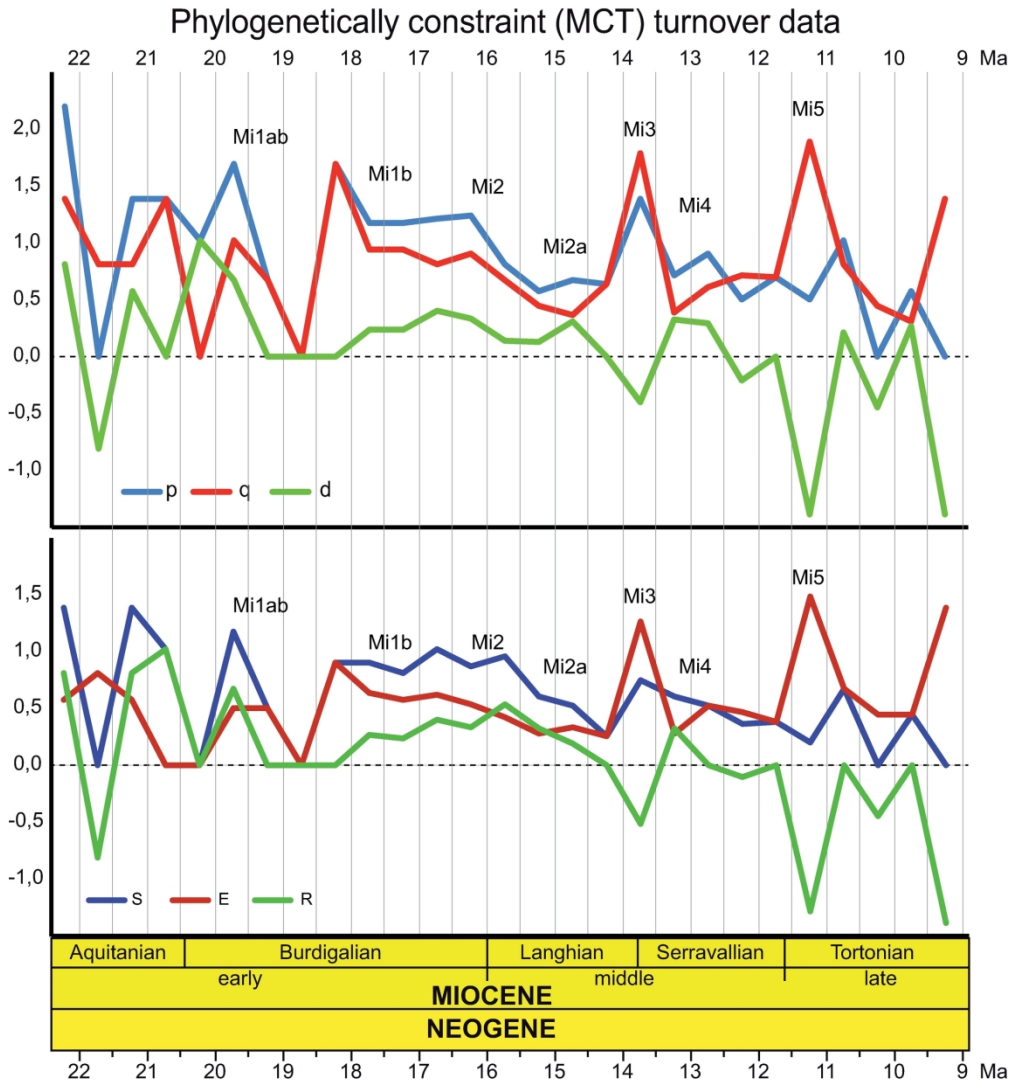

Figure 4. Instantaneous per-capita (top) and deterministic (bottom) rates for Cricetodontinae speciation (p, S), extinction (q, E), and biodiversity change (d, R) calculated using phylogenetically constrained species ranges. Miocene cooling events against geological time are indicated as Mi.

189x205mm (300 x 300 DPI)